Thin-plies in adhesively bonded carbon fiber reinforced polymers

Kupski, Julian; Zarouchas, Dimitrios; Teixeira de Freitas, Sofia

DOI
10.1016/j.compositesb.2019.107627

Publication date
2020

Document Version
Final published version

Published in
Composites Part B: Engineering

Composites Part B 184 (2020) 107627

Contents lists available at ScienceDirect

Composites Part B

journal homepage: www.elsevier.com/locate/compositesb

Thin-plies in adhesively bonded carbon fiber reinforced polymers

Julian Kupski, Dimitrios Zarouchas, Sofia Teixeira de Freitas *

Structural Integrity & Composites Group, Faculty of Aerospace Engineering, Delft University of Technology, Kluyverweg 1, 2629HS, Delft, the Netherlands

ARTICLE INFO

Keywords:
Thin-ply composites
Damage tolerance
Acoustic emission
Joints/joining

ABSTRACT

The aim of this study is to evaluate the enhanced off-axis properties of thin plies to improve the performance of adhesively bonded carbon fiber reinforced polymers. Single lap bonded joints with three different ply thicknesses of 200 μm, 100 μm and 50 μm were tested under quasi-static tensile loading. Acoustic Emission and Digital Image Correlation were used to monitor the damage and strain evolution of the overlap area during testing. 3D post-mortem failure analysis of the fracture surfaces were performed using a 3D profiling microscope. Experimental results show an increase of 16% in the lap shear strength and an increase of 21% in the strain energy when using the 50 μm instead of 200 μm ply thicknesses. However, Acoustic Emission measurements show that the damage initiation is postponed up to a 47% higher load when using 50 μm instead of 200 μm ply thicknesses. Moreover, the total amount of acoustic energy released from initiation up to final failure was significantly less with thin plies. A non-linear finite element analysis up to damage initiation indicates that with decreasing ply thickness, the damage onset inside the composite is postponed to higher loads and moves away from the adhesive interface towards the mid-thickness of the adherend. It is found that, decreasing the single ply thickness of laminated composite adherends in a single overlap bonded joint increases the maximum load and delays damage initiation of the joint, however the damage progression till final failure is more sudden.

1. Introduction

Adhesive bonding is one of the key joining technologies for efficient light weight composite structures. Nevertheless, local peel stresses, generally induced by the specific joint design such as in a single overlap joint (SLJ), lead to inter- or intra-laminar failure inside the composite. Ultimately, this leads to early and sudden failures at lower joint strengths in comparison with their metal counter-parts, where failure occurs inside the adhesive. This drawback in using Carbon Fiber Reinforced Polymers (CFRP) in adhesively bonded joints is hindering their performance and efficiency in full-scale structures where joints are essential.

Thin-plies can represent a promising approach to improve the performance of adhesively bonded CFRP due to their ability to enhance the off-axis performance of composites and postpone delamination. With the development of the fiber tow spreading technology, it is nowadays possible to produce laminates with a very thin single ply thickness, meaning from conventional size (>100 μm) down to about 20 μm [1]. Significant research has been carried out to evaluate the mechanical performance of "thin-plies" in comparison with conventional composites. Camanho at al [2]. experimentally demonstrated that a decrease in ply thickness would lead to a delay of matrix cracking and delamination growth and would therefore enhance the mechanical performance of the composite laminate in their off-axis and out-of-plane directions. Sihn et al. [3] published the first experimental study of composite thin ply laminates in 2007. Uniaxial tensile tests under static and fatigue loading were carried out on unnotched and open-hole specimens. Tests on impact and compression strength after impact (CAI) were also conducted. By analysing stress–strain curves, and by applying several measurement techniques, such as Acoustic Emission (AE), X-ray photography and ultrasonic C-scanning, they observed that micro-cracking, delamination and splitting damage were suppressed in thin-ply laminates under static, fatigue and impact loadings. Yokozeki et al. [4] performed similar experimental studies to prove that the decrease of ply thickness would have an effect on strength and damage resistance of the laminates. Their results show superior characteristics of thin-ply laminates on static tension, tension-tension fatigue, no hole compression strength (NHC), open hole compression strength (OHC) and compression strength after impact (CAI) tests. About 10% increase in OHC and CAI strength was measured with decreasing the ply thickness. In addition, they found a decrease in damage accumulation for thin plies in uniaxial tensile tests using Acoustic Emission (AE) measurement

* Corresponding author. Kluyverweg 1, 2629HS, Delft, the Netherlands
E-mail address: s.teixeiradefreitas@tudelft.nl (S. Teixeira de Freitas).

https://doi.org/10.1016/j.compositesb.2019.107627
Received 30 July 2019; Received in revised form 28 October 2019; Accepted 27 November 2019
Available online 28 November 2019

techniques [4]. Arteiro et al. [5] developed a micro-mechanical finite element model of a composite sub-laminate, in order to accurately represent the micro-mechanical response of composite laminates with thin-plies. The model consisted of a representative volume element of a 90° ply in between two homogenised ±θ° plies. They applied the theory of in-situ strength, which was presented earlier by Camanho et al. [2], to demonstrate that a decrease in ply thickness can be correlated to an in-situ effect, characterised by a reduction in the applied stress needed to extend a transverse crack along the thickness of the ply when the ply thickness increases. Furthermore, the in situ effect plays an important role on the delay of other matrix-dominated failure mechanisms [5]. Amacher et al. [6] followed the work of Yokozeki et al. [4] by their approach of experimental characterization and modelling of size effects. They agreed very well with the early results of Sihn et al. [3], showing that thin ply composites exhibit a significantly delay in damage initiation in comparison with conventional laminates. By using different ply thicknesses, ranging from 30 to 300 g/m^2 in quasi isotropic tensile tests, they identified quasi-brittle failure in the thin plies instead of extensive delamination and transverse cracking patterns in thick plies. Recently, Cugnoni et al. [1] expanded their previous study [6], by evaluating eight different formulations of thin-ply composites ranging from low modulus to high modulus carbon fibres through compression strength after impact (CAI) and open hole tensile (OHT) tests. They concluded that, for thin-ply composites, the maximum strength is limited by the ultimate strain of the fibre. By adding a thermoplastic interlayer toughening component they could show an increase in damage resistance in the thin plies [1].

Extensive literature on composite materials suggests that thin plies delay delamination and matrix cracking. This effect of thin plies can potentially be used to enhance the performance of bonded joints. The goal of this study is therefore to explore the influence of ply thickness on the overall joint strength under quasi-static tensile loading, in particular on the damage initiation, the final fracture surface, the failure load and the released energy. If the use of thin plies can postpone the damage initiation, as shown in literature, this might postpone the damage inside the composite adherend and enhance the performance of composite bonded joints and, therefore, contribute to further promote adhesive bonding in primary composite aerospace structures.

2. Materials and specimens

2.1. Materials

The materials used for this study are unidirectional Prepreg tapes from carbon fibres and epoxy resin in combination with an epoxy film adhesive. The Prepreg material was chosen NTPT-HTS(12K)-5-35%, which is a thermoplastic-toughened epoxy resin unidirectional (UD) Prepreg system. The adhesive was Scotch-Weld™ AF 163-2K in 293 g/m^2 areal weight, including a knit supporting carrier, from 3 M Netherlands B.V. The relevant material parameters are presented in Table 1 and Table 2. All values are valid at room temperature (23 °C). Indices are given for different coordinate directions with "1", "2" and "3" standing for the direction along in-plane longitudinal, in-plane transverse and out-of-plane, and with "T" and "C" standing for "tensile" and "compressive", respectively.

2.2. Specimens

In order to examine the effect of ply thickness on tensile bonded joint strength, the single overlap joint (SLJ) was chosen as the reference design for this study. Three different design configurations were tested in which the SLJ geometry, with overlap length and width of 25.4 mm, was kept constant but the composite laminate adherends ply thicknesses changed. Table 3 shows the three composite adherend configurations, referred to as THICK, MEDIUM and THIN. In order to limit the study to the effect of the single ply thickness, the interface ply angle was kept the same for the three configurations as well as the adherend bending stiffness, ranging from 55 GPa (THIN) to 56.2 GPa (THICK). Based on the classical laminate theory (CLT), the longitudinal bending stiffness was determined as the flexural engineering constant of a laminate given by

$$E_x^f = \frac{12}{D^*_{11} t^3} \quad (1)$$

for symmetric layups, with D^*_{11} being the first row/first column entry of the resulting inverse of the bending stiffness matrix, t being the overall laminate thickness and x corresponding to the direction along the SLJ-length (longitudinal direction) [13].

Five specimens have been built per test configuration in accordance with ASTM-D-5868 [14]. All adherend laminates have been manufactured from the same Prepreg roll, with 32 layers of a single ply thickness of 50 μm, adding up to 1.6 mm total adherend thickness. The MEDIUM and THICK configuration were built by stacking blocks of 2 plies and 4 plies of the same ply angle, respectively. In this way an increase in ply thickness is achieved by the ply blocks, see Table 3. The idea of stacking ply blocks has already been introduced by Sihn et al. [3] and is a common method for creating specimens of different ply thickness from the same Prepreg roll.

Composite adherends were laminated in a Prepreg hand layup process, with 5–10 min of de-bulking at an under pressure lower than 100

Table 1
Material properties of NTPT-HTS(12K)-5-35% for a UD-Prepreg layer.

Longitudinal tensile strength	X_T	2180 MPa[a]
Longitudinal compressive strength	X_C	1057 MPa[a]
Transverse tensile strength	Y_T	81 MPa[a]
Transverse compressive strength	Y_C	255 MPa[c]
Longitudinal tensile modulus	E_{11T}	85630 MPa[a]
Transverse tensile modulus	$E_{22T} = E_{33T}$	9060 MPa[a]
In-plane shear modulus	$G_{12} = G_{13}$	5000 MPa[b]
Transverse shear modulus	$G_{23} = E_{33T}/(2(1+\nu_{23}))$	3485 MPa
In-plane shear strength	$S_{12} = S_{13}$	81 MPa[b]
Transverse shear strength	S_{23}	35 MPa[c]
In-plane Poisson ratio	$\nu_{12} = \nu_{13}$	0.27[c]
Transverse Poisson ratio	ν_{23}	0.30[c]

[a] Based on material characterization tests, ASTM D3039/D3518/D6641 [7–9].
[b] TDS of NTPT Thinpreg™ 135 with HS40/T800 carbon fibers in 67 g/m^2 [10].
[c] Camanho et al. [2].

Table 2
Material properties of Hysol AF163-2 epoxy film adhesive.

Tensile strength	X_{Adh}	46 MPa[a]
Maximum elongation at break	ε_{tmax}	5.4 %[a]
Tensile modulus	E_{Adh}	2043 MPa[a]
Poisson ratio	ν_{adh}	0.34[b]

[a] Teixeira et al. [11].
[b] TDS of Scotch-Weld™ AF 163-2K 293 g/m^2 [12].

Table 3
Three test configurations with different ply thickness, by means of ply blocks of 2 layers for the MEDIUM and 4 layers for the THICK configuration.

Design configuration	Stacking sequence	Equivalent longitudinal bending stiffness [GPa]	UD ply thickness [mm]
THICK (Ply block of 4 plies)	$[(45)_4/(0)_4/(-45)_4/(90)_4]_s$	56.6	4 × 0.05 = 0.20
MEDIUM (Ply block of 2 plies)	$[(45)_2/(0)_2/(-45)_2/(90)_2]_{2s}$	56.6	2 × 0.05 = 0.10
THIN (Single ply)	$[45/0/-45/90]_{4s}$	55.0	1 × 0.05 = 0.05

mbar between every fourth layer. The laminates were placed between a base plate of 12 mm thickness and a caul plate of 2 mm thickness from 2024-T3 aluminium alloy. An autoclave curing process comprised a single dwell step at 177 °C and 5 bar gauge pressure, with 800 mbar under pressure inside the vacuum bag for 120 min time. In order to minimize resin flow-out along the edges of the laminate, aluminium barriers were added.

Fig. 1 shows optical microscopy images, Carl Zeiss AxioCam ECr 5s with 10x magnification, of the cross sectional cut of the three laminates with different ply thickness configurations after curing. The thickness of different ply blocks per configuration is visible. For the THICK configuration, the ply block of 4 layers can be identified as well as the symmetry line of the stacking sequence with 8 layer (2 times ply block). Correspondingly, for the MEDIUM configuration, the ply block of 2 layers and the symmetry line with 4 layers (2 times ply block) can be identified. Finally for the THIN, the single layers and the symmetry lines are visible. The interface between the layers within one ply block is hardly noticed. Therefore, it is reasonable to consider a ply block as a single UD layer with increased thickness.

2.3. Surface treatment

A suitable surface treatment prior to bonding was chosen as combination of degreasing the surface with Acetone and a 7 min long exposure to UV light inside an ozone containing atmosphere. The procedure was performed according to previous studies that showed good CFRP surface wettability after applying the same treatment [15–17].

The efficiency of the surface treatment was evaluated by measuring the contact angle of a 4 µl distilled water, using the Technex Cam200/Attension Theta V4.1.9.8 system. The value of this contact angle reduced by 78.9%, from 101.3° (±1.3°), before treatment to 21.3° (±0.9°), after treatment, for all configurations. These values are in accordance with literature and correspond to a good wettability of the surface [17].

2.4. Bonding

The uncured film adhesive was placed onto the treated surface of the cured adherends and a vacuum setup was arranged around it for bonding. The curing process was performed in an autoclave at 2 bar gauge pressure and 120 °C curing temperature for 90 min dwell time, venting the vacuum bag to full atmosphere. After the bonding process, the average bond line thickness was 141 µm (±26 µm), which deviates by 6% from the manufacturer's TDS of 150 µm. This is considered within acceptable tolerance. Excess adhesive gathered at the bond line tips and formed a small fillet at the edges.

3. Experimental analysis

3.1. Experimental setup

Five specimens per layup configuration were subject to quasi-static tensile loading, in accordance with ASTM standard D 5868-01 [14]. The tests were set as displacement controlled with a constant displacement rate of 1.3 mm/min. Tests were performed on a Zwick-Roell Allround Line Z250 SW testing machine with a load cell of 250 kN. Fig. 2 illustrates a schematic representation of the test setup. The specimen was held by two clamps at 250 bar hydraulic pressure. The initial distance of the clamps was set at 200 mm, with a misalignment of 1.8 mm to counterbalance the overlap offset. A mechanical extensometer, BTC-EXMACRO.H02 by Zwick-Roell/testXpert II, captured the elongation between two points of 60 mm distance, adjacent to the overlap area. Additionally, the strain field of the overlap area was monitored using digital image correlation (DIC) technique. For this, the VIC-3D™ system by Correlated Solutions, Inc. was used at a 1 Hz frame capture speed. In order to monitor the damage events of the specimens, an acoustic emission (AE) system by Vallen Systeme GmbH was employed, consisting of two VS900-M sensors, which were attached onto the same side of the specimen at ± 42.5 mm from the overlap centre and connected to the AEP4H 34 dB amplifier.

3.2. Load-displacement

Fig. 3a) shows typical load-displacement curves for the three different ply thickness configurations. The maximum load ranges (in average) from 16.1 kN for the THICK to 18.5 kN for the THIN configuration, which is an increase of 15% with decreasing ply thickness. The average lap shear strength (σ_{LSS}) in Fig. 3b) is derived by dividing maximum load (P_{max}) over the bonded area for each specimen, given by the bond line length multiplied by the specimen width. The results show an increase of 16% in average lap shear strength when comparing THICK to THIN ply thickness configuration.

In addition, the strain energy under the load-displacement curve allows a comparison of average energy until failure for the three different ply thickness configurations. This has been derived determining the area under the load-displacement curve using a trapezoid rule. The result is presented in Fig. 3c), indicating a 21% increase in strain energy for the THIN in comparison with the THICK ply thicknesses. Table 4 summarizes the results.

3.3. Acoustic emission

Fig. 4 and Table 4 present the results from AE-monitoring recorded during tests. On the left hand side, in Fig. 4a)–c), the cumulative AE-hits (left axis) and the recorded load (right axis) are plotted over the displacement for the three different configurations, THICK, MEDIUM and THIN, respectively. On the right hand side in Fig. 4d)–f) the cumulative energy (left axis) and the load (right axis) are plotted over the displacement.

All AE hit plots on the left side of Fig. 4 start with a linear line with a small slope. At a certain displacement ("knee-point"), the number of hits increases significantly such that the line continues with a steeper slope. This trend is typical for all configurations. The point where the plots

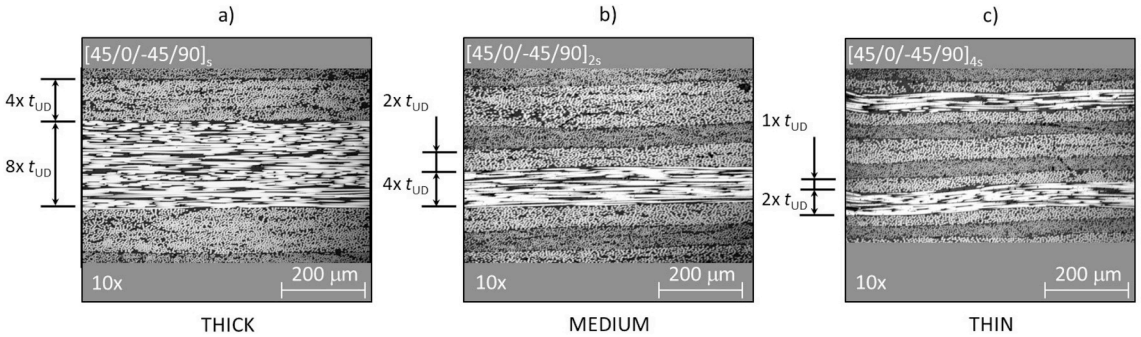

Fig. 1. Cross sectional cut of laminates with different ply blocks, optical microscopy images, Carl Zeiss AxioCam ECr 5s with 10x magnification.

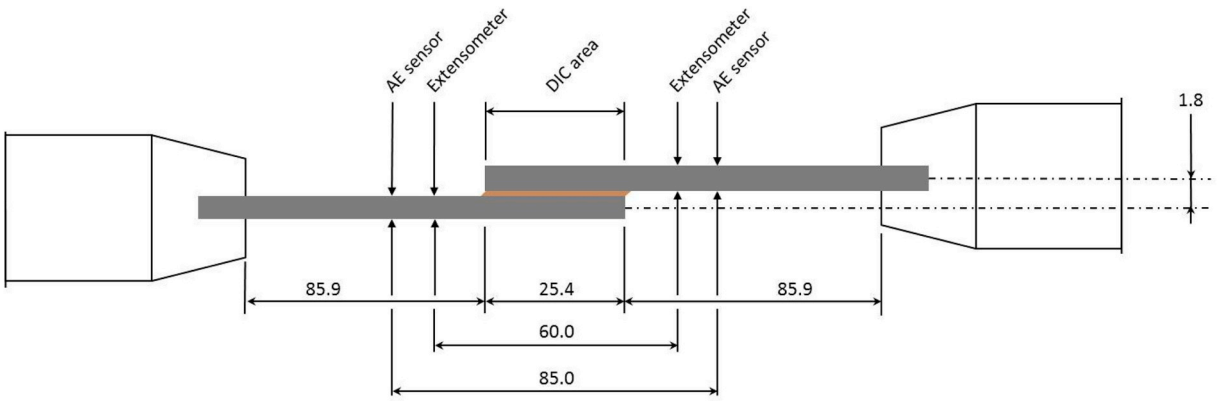

Fig. 2. Test setup for static tensile loading, dimensions in [mm].

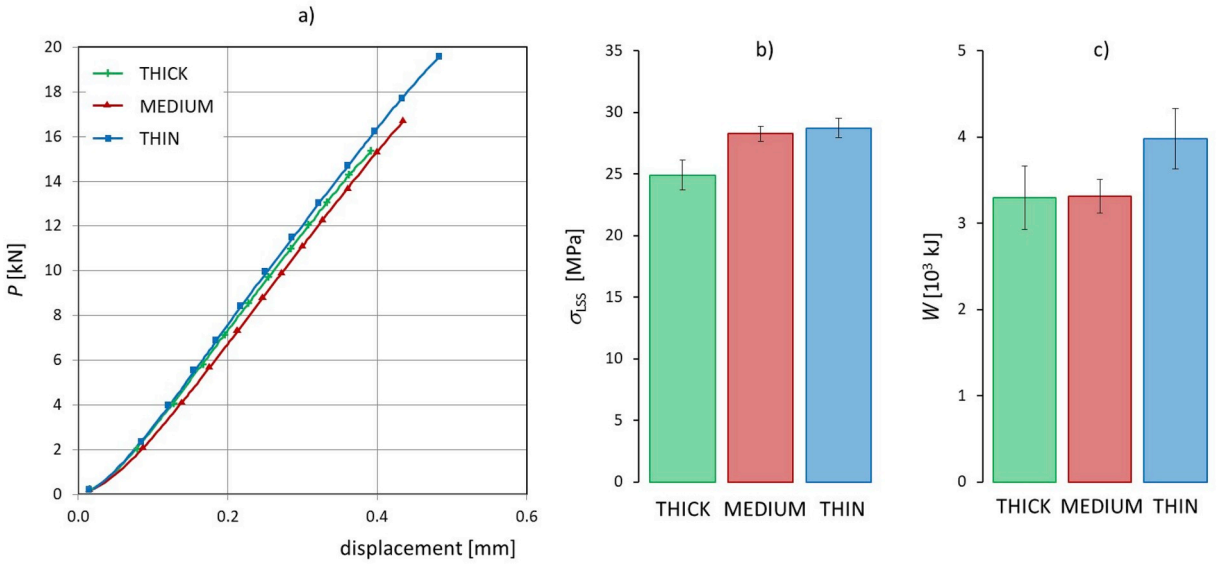

Fig. 3. a) Typical load displacement curves, b) average lap shear strength (σ_{LSS} ± standard deviation) and c) strain energy (W ± standard deviation) for the three different ply thickness configurations.

Table 4
Maximum load (P_{max}), lap shear strength (σ_{LSS}) and energy (W), load/displacement at damage initiation, based on cumulative AE energy release, for the three different ply thickness configurations (average (±standard deviation)).

Design	THICK	MEDIUM	THIN
Maximum load P_{max} [kN]	16.1 (±0.8)	16.9 (±0.4)	18.5 (±0.7)
Lap Shear Strength σ_{LSS} [MPa]	24.9 (±1.2)	28.3 (±0.6)	28.8 (±0.8)
Strain energy W [10^3 kJ]	3.3 (±0.4)	3.3 (±0.2)	4.0 (±0.4)
Load at damage initiation [kN]	11.1 (±0.8)	13.5 (±0.9)	16.3 (±1.5)
Displacement at damage initiation [mm]	0.28 (±0.02)	0.35 (±0.01)	0.40 (±0.04)
Cumulative AE hits	2063 (±469)	847 (±149)	826 (±281)
Cumulative AE energy [J]	162.8 (±41.9)	41.3 (±12.9)	8.5 (±4.3)

change to a steeper slope is believed to indicate damage initiation inside the specimen. Comparing the cumulative number of AE-hits on the left side, Fig. 4a)–c), with the cumulative AE-energy on the right side, Fig. 4d)–f), the significant change of the plots is more pronounced in the later. The AE-hits in the initial slope region have no significant energy, and seem to accumulate energy only after the knee point. Therefore the plots of Fig. 4d)–f) are used to obtain the load at which damage first initiates, proposing the following criterion:

$$E^{AE}{}_i > 0.10 \times 10^{-12}\ \text{J AND}\ E^{AE}{}_{i+1} \geq 2\ \text{x}\ E^{AE}{}_i \quad (2)$$

with $E^{AE}{}_i$ being the acoustic energy per hit, recorded at 1 Hz frame rate. The criterion was set to be consistent for all cases.

Based on the results, it can be observed that, the displacement at which damage initiation is believed to occur, is postponed to higher values when decreasing the ply thickness. The number of hits as well as the cumulative AE-energy after this knee point are significantly reduced for the THIN ply configuration. However, on the number of hits, in Fig. 4a)–c), this difference is more visible between the MEDIUM and THICK configuration than between the MEDIUM and the THIN. The final cumulative energy, in Fig. 4d)–f) changes significantly between the configurations, in average from 163 × 10^{-12} J in case of the THICK down to 9 × 10^{-12} J for the THIN configuration. At the same time, the displacement at damage initiation increases from 0.28 mm up to 0.40 mm when comparing the THICK to the THIN configuration. By comparing the position of the knee point for the three different ply thickness configurations, it can be concluded, that the damage initiation is postponed to 47% higher loads with decreasing ply thickness. Table 4 summarizes maximum load as well as load and displacement at damage initiation in comparison with the total amount of cumulative hits and

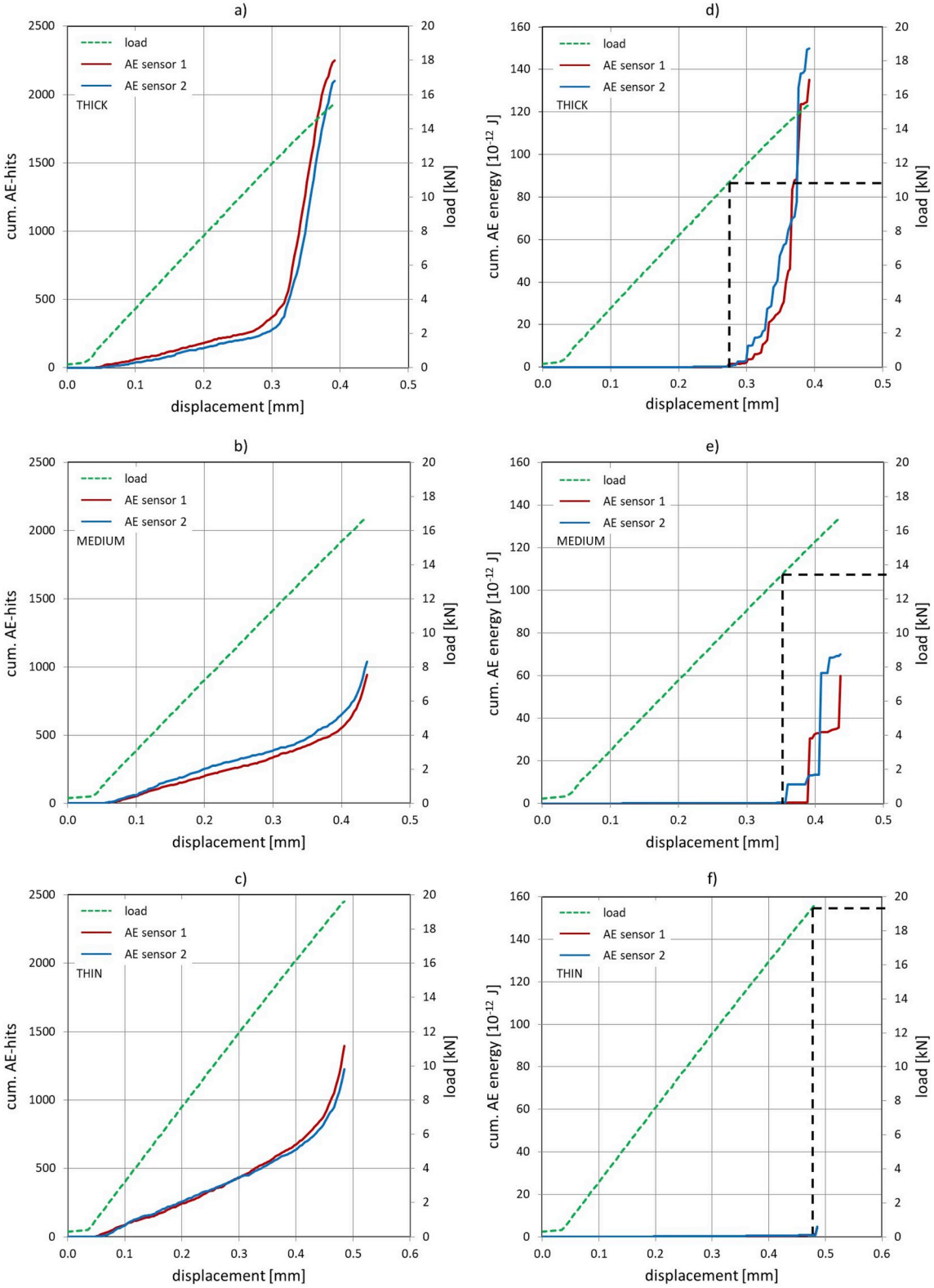

Fig. 4. Typical measurements of cumulative acoustic hits [−] a)-c) and cumulative acoustic energy [10^{-12} J] d)-f) for the three different ply thickness configurations.

AE-energy, for the three different ply thickness configurations. The cumulative AE energy per configuration was thereby derived in two steps: Firstly, the final cumulative energy of each of the two sensors was averaged for each specimen. Secondly, the cumulative AE energy was averaged over all specimens per configuration.

3.4. Fracture surfaces

Fig. 5 shows typical fracture surfaces of the different ply thickness configurations. The fracture surfaces show that the failure occurred partly inside the composite and partly inside the adhesive. However, in all cases the composite failure clearly dominates the final fracture

surface.

A comparison of the three configurations reveals that the final fracture surface spreads over a larger area with increasing UD-ply thickness. The difference in total fracture surface between the configurations is quantified in Table 5, being A_f^{comp} and A_f^{coh} the area of the fracture surface inside the composite adherend, and inside the adhesive, respectively, A_f^{total} the total area of the fracture surface and A_{OL} the overlap area. On average, the total fracture surface in the THICK configuration is of 760 mm^2, decreasing to 668 mm^2 for the MEDIUM and to 637 mm^2 for the THIN configuration.

In Fig. 6, the portion of composite versus cohesive failure is plotted for each ply thickness configuration. Comparing the three areas of cohesive failure, there is no visible trend. An average cohesive fracture surface area of 38 mm^2 for the THICK decreases to 17 mm^2 for the MEDIUM and increases again to 30 mm^2 for the THIN configuration. Comparing the area of cohesive versus total failure, the THICK configuration resembles 5.1% cohesive failure, while the MEDIUM contains 2.6% and the THIN 4.7% of the fracture inside the adhesive.

Post mortem fracture surface analysis was performed using the Keyence VR5000 Wide-area 3D profiling system. Fig. 7 shows the bottom side of a typical THICK configuration (Fig. 5a). The final fracture surface is presented as a 3D profile. A cross section profile along the length of the overlap is also shown below the 3D profile. This height profile throughout the overlap region gives an idea where the crack has travelled through the laminate. Fig. 8 and Fig. 9 show the 3D- and the height profile along the overlap length for the typical MEDIUM and the THIN configuration. The ply thickness t_{UD} represents the single layer thickness in case of the THIN but the total thickness per ply block, in case of the MEDIUM and THICK configurations. The experimental ply thickness deviates from the nominal values of Table 3 by about 10%.

In the THICK configuration, in Fig. 7, the crack progresses partly inside the first 45° ply block of the top adherend, and partly inside the adhesive bond line. A similar crack propagation is visible in the cross-section cut of the MEDIUM configuration, in Fig. 8. However, in Fig. 9, there are several steps inside the composite laminate of the upper adherend visible in the final fracture surface of the THIN configuration.

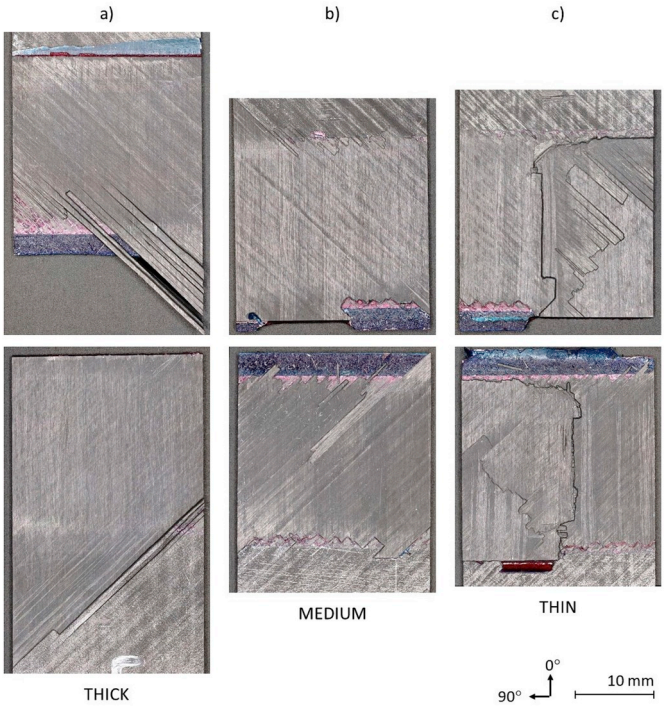

Fig. 5. Typical fracture surfaces for each ply thickness configuration after final failure.

Table 5
Fracture surface analysis for the three different ply thickness configurations average(±standard deviation).

Design	THICK	MEDIUM	THIN
A_f^{comp} [mm^2]	721 (±59)	651 (±19)	607 (±265)
A_f^{coh} [mm^2]	38 (±25)	17 (±9)	30 (±145)
$\frac{A_f^{coh}}{A_f^{comp}+A_f^{coh}}$[%]	5.1 (±3.0)	2.6 (±1.3)	4.7 (±2.2)
$\frac{A_f^{total}}{A_{OL}}$[%]	117.8 (±9.5)	103.5 (±1.9)	98.8 (±4.2)

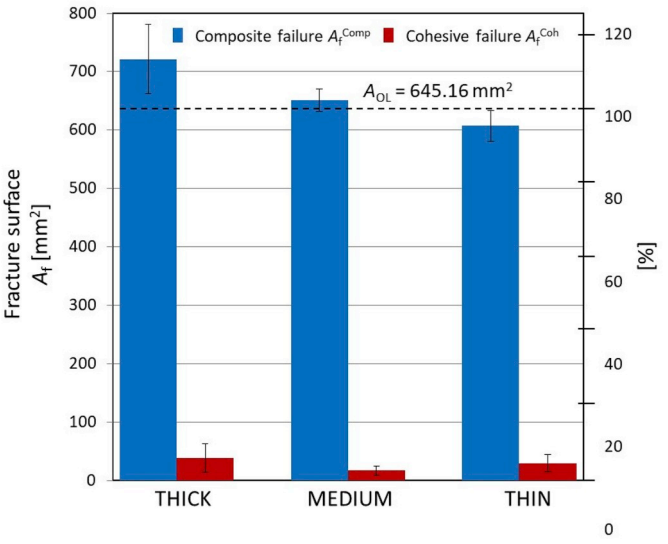

Fig. 6. Typical fracture surfaces for each ply thickness configuration after final failure.

Two paths are plotted along the overlap length. In the path A-B, the crack overcomes multiple laminae and reaches up to the 10th layer away from the adhesive bond line, propagating in the longitudinal (in-plane) direction. After 30% of overlap length, the crack path changes to transverse (out-of-plane) direction, dropping through the thickness of the adherend, and continues in the longitudinal (in-plane) direction along the interface of the 6th and 7th ply. In the second path C-D, the final fracture surface was identified on the interface between 1st and 2nd layer. In all three cases, the fracture surface tends to locate near the interface between a 0°- and a 45°-ply.

It is important to notice that, for the THICK and MEDIUM configurations the crack, despite apparently intralaminar within 45 ply block, seems to propagate preferably at the interface between two 45°-plies, which would actually mean interlaminar failure. This is no longer the case for the THIN (no ply blocks), where the crack path is along the 0/45-interface. In the cross-sectional images of THICK and MEDIUM shown in Fig. 1, the interface within a ply block is much less pronounced than the interface between plies of different orientation, due to nesting effects. Nevertheless, the crack path for THICK and MEDIUM seems to be affected by the interface of the ply blocks, as commented previously. The fracture patterns could potentially be different if the different ply thicknesses were achieved by producing plain plies of different thicknesses instead of a ply block.

4. Numerical analysis

4.1. Numerical model

A finite element analysis (FEA) of the SLJ geometry under tensile loading was performed with the commercial software Abaqus 2017. The

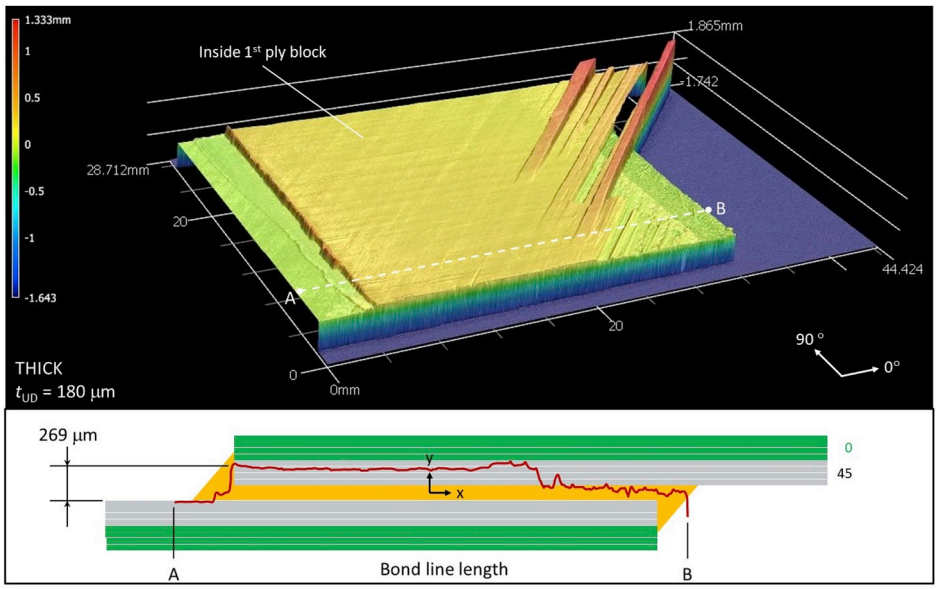

Fig. 7. Final fracture surface of a typical THICK configuration.

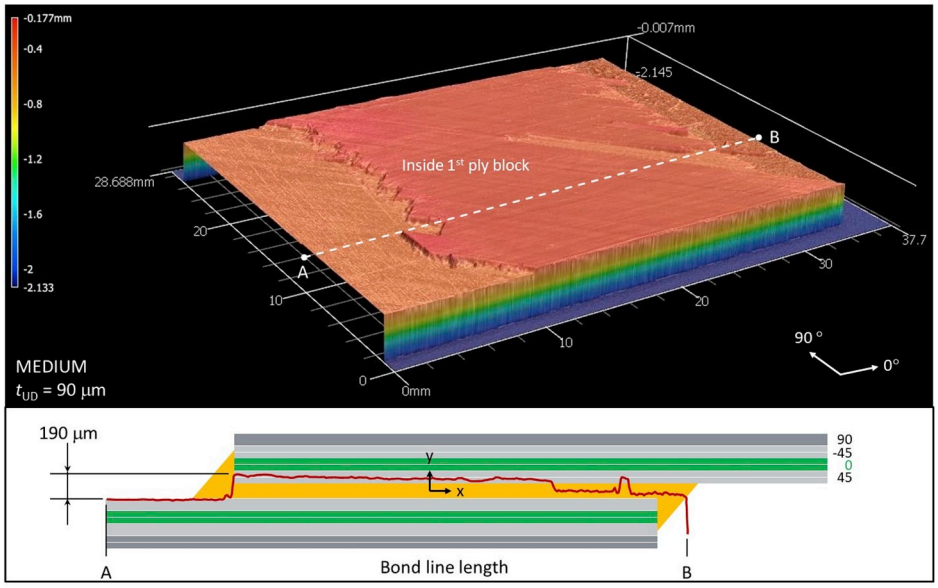

Fig. 8. Final fracture surface of a typical MEDIUM configuration.

purpose of this FEA was to numerically simulate the experimental tests up to damage initiation. An implementation into a 3D model gives insight into the stress field around the bond line, aiming to capture load and location of damage initiation and help to interpret the resulting failure mechanisms. The composite was modelled as linear elastic, based on the properties listed in Table 1, while the adhesive was modelled linear-elastic/plastic, using the values from Table 2. The bond line thickness was modelled with 150 µm, (nominal thickness).

The load was applied in a single step with 6 load increments taking into account non-linear geometry effects. The specimen between the clamps was simulated using continuous 3D solid elements with reduced integration (C3D8R). Fig. 10 illustrates the model with the specimen's dimensions, boundary conditions and mesh. At the right side all nodes inside the cross-sectional surface are blocked in 3 Degrees of Freedom (DoF), while on the left side, solely longitudinal displacement is allowed (x-direction).

The region around the left overlap edge is highlighted in Fig. 11. The spew fillet geometry is an approximation of its experimental counterpart. All specimens of this study had a spew fillet shape similar to a 45° triangle. In all cases, the spew fillet reached at least up to half of the adherend's height (= 0.8 mm). Based on this, it was decided to model a triangular fillet shape of 45° slope reaching up half the adherend's height, as a good approximation to represent the specimens within this study.

4.2. Mesh convergence

To guarantee that the results were mesh independent, a mesh convergence study was performed. In Fig. 12, the peel stress (σ_{yy}) is plotted along the overlap length, from left to right, including the length of both fillets in Fig. 12a), and through the thickness of the overlap left edge, from bottom to top in Fig. 12b). Both paths are situated in the centre of the joint in width direction. The length and width of one element in the overlap tip region is set to 100 µm, while the thickness of

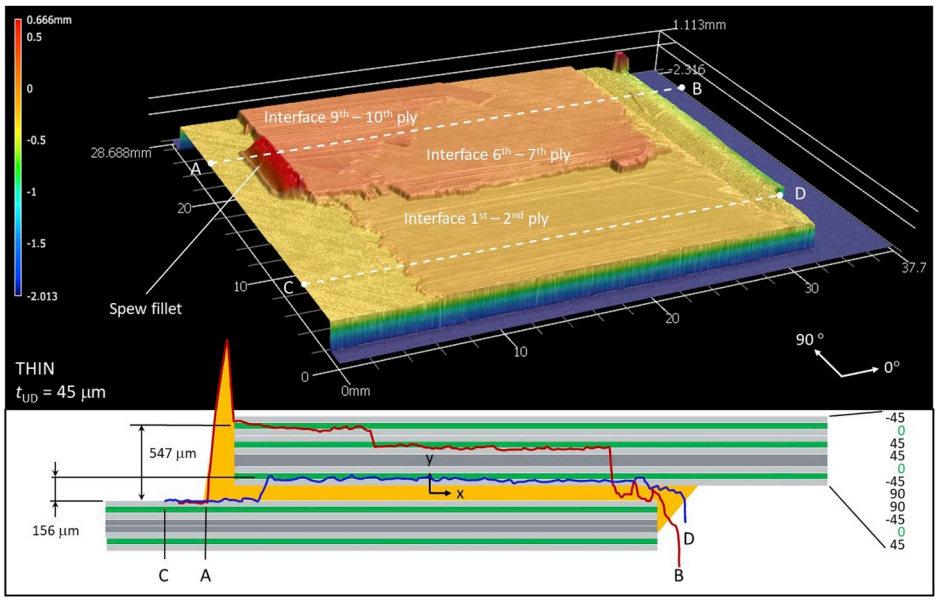

Fig. 9. Final fracture surface of a typical THIN configuration.

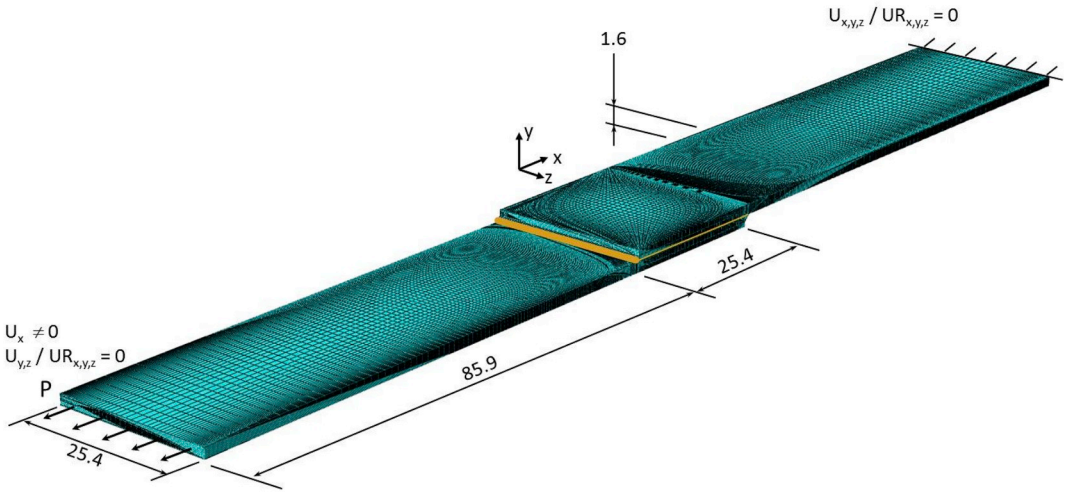

Fig. 10. 3D FE-model between the clamps with specimen dimensions in [mm], and boundary conditions.

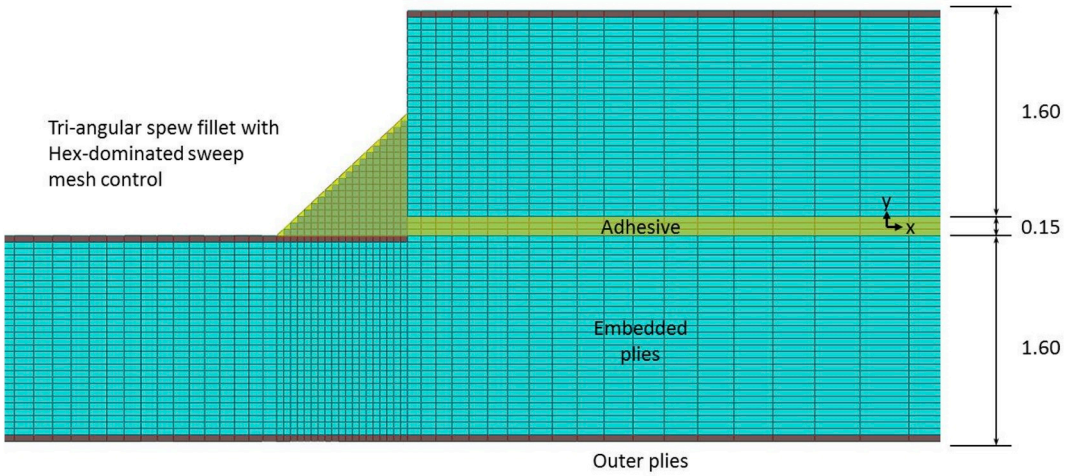

Fig. 11. Zoom on overlap region with triangular spew fillet and material section assignments, all dimensions in [mm].

one element corresponds to one UD ply thickness of 50 μm, throughout the whole model. In order to avoid showing the stress jumps at the interface, the path in Fig. 12a) was chosen exactly in the middle of the bond line and in Fig. 12b) 5 μm inwards of the overlap end, in x-direction.

Mesh 1 is composed of 3D cubic elements with 8 nodes (linear interpolation) and reduced integration (one integration point at the centre of the cube). These elements in ABAQUS are referred to as C3D8R. The dimensions of Mesh 1 (C3D8R in green) in Fig. 12a) were based on the smallest element size at the bond line region with the dimensions length = 100 μm, width = 100 μm and height = 50 μm. Towards the clamps the size of the elements is gradually increased, leading to 921,344 elements of type C3D8R in total. Mesh 2 is a mesh refinement of Mesh 1. The refinement has been performed in two ways: (1) by increasing the number of elements in the overlap region, leading to a total number of 2,036,516 elements and (2) by increasing the number of integration points within one element from 1 to 8, choosing a 3D-solid element with linear interpolation of type C3D8 with no reduced integration (8 integration points) (Mesh 2 in red).

As can be seen in Fig. 11, the mesh refinement (Mesh 2 in comparison with Mesh 1) affects the stress distribution around the tip of the overlap. A difference in maximum stress values of 4.6% in Fig. 12a) and 6.5% in Fig. 12b) was considered a sufficient convergence with the coarser Mesh 1 of 921,344 elements of type C3D8R. All results presented in this study are therefore based on Mesh 1.

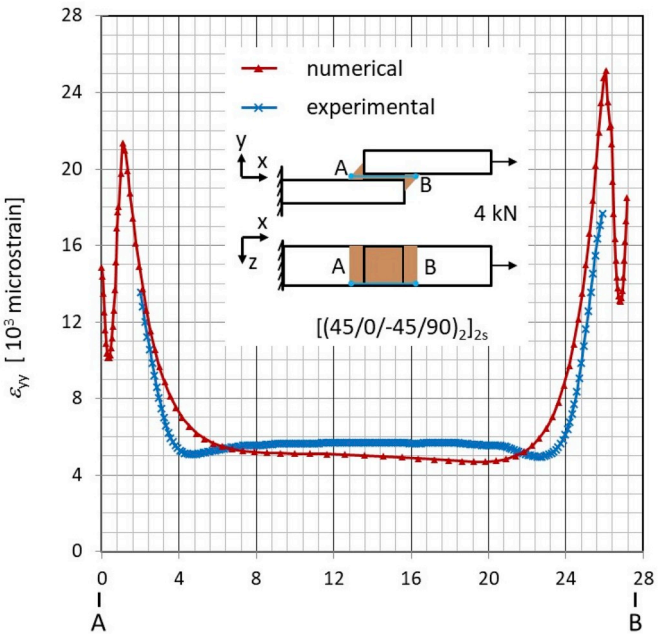

Fig. 13. Peel strain(ε_{yy}) along the bond line in [10^3 microstrain], numerical versus experimental method.

4.3. Validation of numerical model

In order to validate the numerical simulations, the strain distribution measured during test by means of DIC is compared with numerical results. Fig. 13 shows a representative example of the peel strain distribution along the mid-thickness of the bond line. In width direction, the paths is set along the edge of the bond line, where the strains from the DIC are recorded. The presented values correspond to the design configuration with MEDIUM ply thickness of 100 μm and layup $[(45)_2/(0)_2/(-45)_2/(90)_2]_{2s}$ at a reference load of 4.064 kN. This value has been chosen to make sure the comparison is performed before damage initiation occurred in the test.

Overall, the numerical analysis agrees well with the experimentally measured strain distribution. However, there are some deviations between the plots towards the bond line tips. This is believed to be caused by two main reasons: 1) the strain field captured by the camera is representing the strain of the colour coating, that was applied to provide a contrast rich speckle pattern, as common for DIC systems and therefore some discrepancy between these and the real adhesive strain is expected; and 2) due to the quite small adhesive bond line thickness of 141 μm, the method to extract strain values via image correlation software Vic3D 7 by Correlated Solutions, is prone to inaccuracy when picking the peel strain (ε_{yy}) visualization path, that may not exactly match the same location as that of the numerical model.

Moreover, Fig. 13 also shows an asymmetry of the numerical strains at the edges. This asymmetry decreases significantly towards the mid-width of the specimen. This effect is believed to occur due to a layup related reason: The laminate is not antisymmetric, so that, according to the given CLT theory, the entries D16 and D26 of the ABD matrix have values unequal zero [13]. This instance leads to a bending-twisting coupling inside the laminated adherends. The offset between the

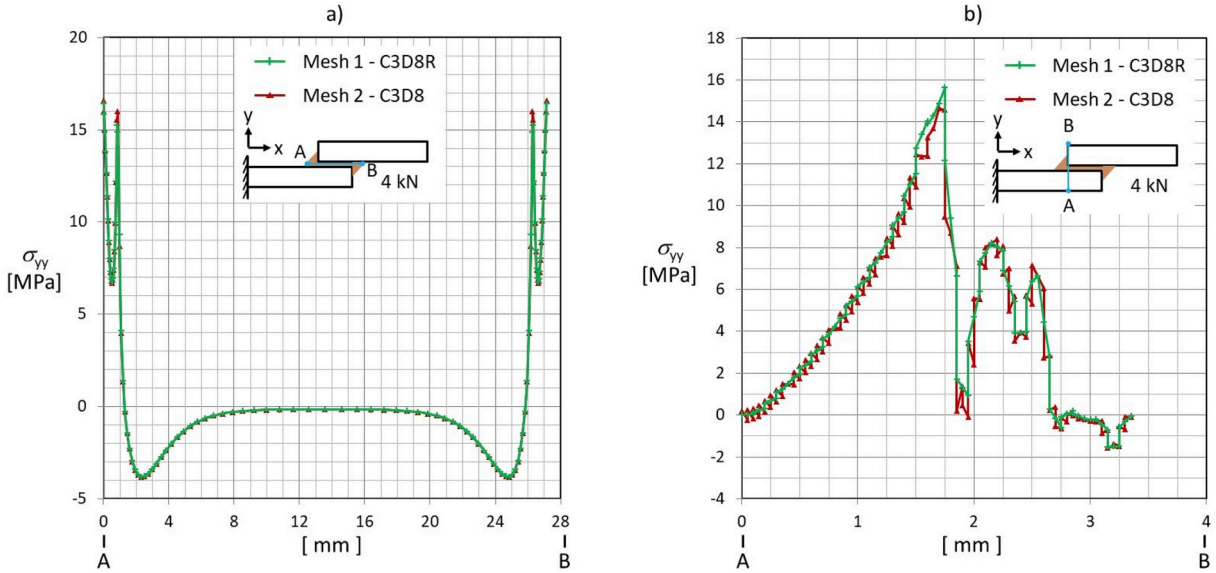

Fig. 12. Mesh convergence study on peel stress (σ_{yy}) distribution along overlap length a) and through bond line thickness b).

adherends due to the SLJ geometry causes an inevitable momentum of secondary bending, which induces a twist to the joint, consequently translating into a difference in peel stress between the left and right bond line tip.

Nevertheless, this asymmetry of the strain values along the bondline decreases with decreasing the ply thickness. This variation in asymmetry between the three configurations (highest for the THICK and lowest for the THIN) may influence the global joint behaviour but it marginally affects the peak peel and shear stress values at damage initiation or at final failure.

4.4. Numerical results

Once the numerical analysis is validated, it can be further explored to study the stresses around the overlap region. Fig. 14 presents the shear (τ_{xy}) and peel (σ_{yy}) stress distribution along the bond line length for all layup configurations given by the numerical model at a pre-defined load of 4.064 kN. None of the tested specimens indicated any significant amount of AE hits nor accumulated AE energy up to this load. Therefore, the value was set in order to stay within region before damage initiation. The plot path is taken at centre position in width direction of the joint and mid-thickness of the bond line. The results show almost identical stresses along the bond line for the three configurations, both in shear (τ_{xy}) and peel (σ_{yy}).

In Fig. 15, plots are taken at centre position in width and cover the complete overlap thickness of 3.35 mm length from bottom to top. Fig. 16 gives, a closer look of the same stresses near the region of the adhesive bond line.

Fig. 15 shows that stresses vary inside the composite adherends depending on the ply thickness, while remaining again almost identical inside the adhesive. The shear stress (τ_{xy}) distribution in Fig. 15a) differs significantly, while the peel (σ_{yy}) stress plots in Fig. 15b), are more consistent for the different ply thickness configurations. This effect is related to the ply thickness, or in fact to the different stacking sequences of the THIN, MEDIUM and THICK configuration in Table 3. As shown in previous work from the authors [18], the fiber orientation does not have a large influence on the out-of-plane peel stress distribution inside the adherend, while for the shear stresses, as an in-plane stress, the fiber orientation has a significant influence on its stress distribution.

As stated in Table 3 of subsection 2.2, the equivalent laminate bending stiffness of the adherends as well as the outermost layer in contact with the adhesive are kept constant throughout the test design. Therefore global and local stiffness of the adherends remain constant and the adhesive experiences the same peel and shear stresses in all three configurations.

Looking closer onto Fig. 16, the maximum (σ_{yy}) and shear (τ_{xy}) stress are situated at different locations inside the joints: Both the shear (τyx) and peel (σyy) stress have their maximum at the interface between the outermost 45° layer and the adhesive, towards the upper adherend. This point is indicated in Fig. 16a) and b) with the right dashed line. Inside the adhesive, the maximum shear (τyx) stress is at the centre of the adhesive in through-thickness direction. The maximum peel (σyy) stress, however, is more pronounced towards the interface with the upper adherend, Fig. 16a) and b), right dashed line. These observations for maximum (σ_{yy}) and shear (τ_{xy}) stress are consistent for all three configurations. Therefore, it can be concluded that, a different adherend ply thickness does not have and influence in the location of stress hot spots inside the adhesive, when looking through the thickness at the tip of the bonded region.

5. Discussion

5.1. Sentry function

A correlation of the AE-data and load-displacement curves can give more insights into the damage characterization. One method, which is used for this correlation, is called Sentry function [19]. The sentry function is the natural logarithm of the ratio between mechanical and acoustic emission energies, reading:

$$f(x) = ln\frac{E_s(x)}{E_a(x)} \tag{3}$$

where $E_s(x)$, $E_a(x)$ and x are the strain energy, the AE energy and the displacement, respectively. The strain energy is taken as the area under the load-displacement curve whereas the AE energy is the summation of each wave's energy. Depending on the material damaging progression, the Sentry function behaviour can take any combination of the following four trends:

- Type I (P_I (x)): Increasing trend, representing a strain energy storing phase
- Type II (P_{II} (x)): A sudden drop of the function which may be related to a significant internal material failure occurrence

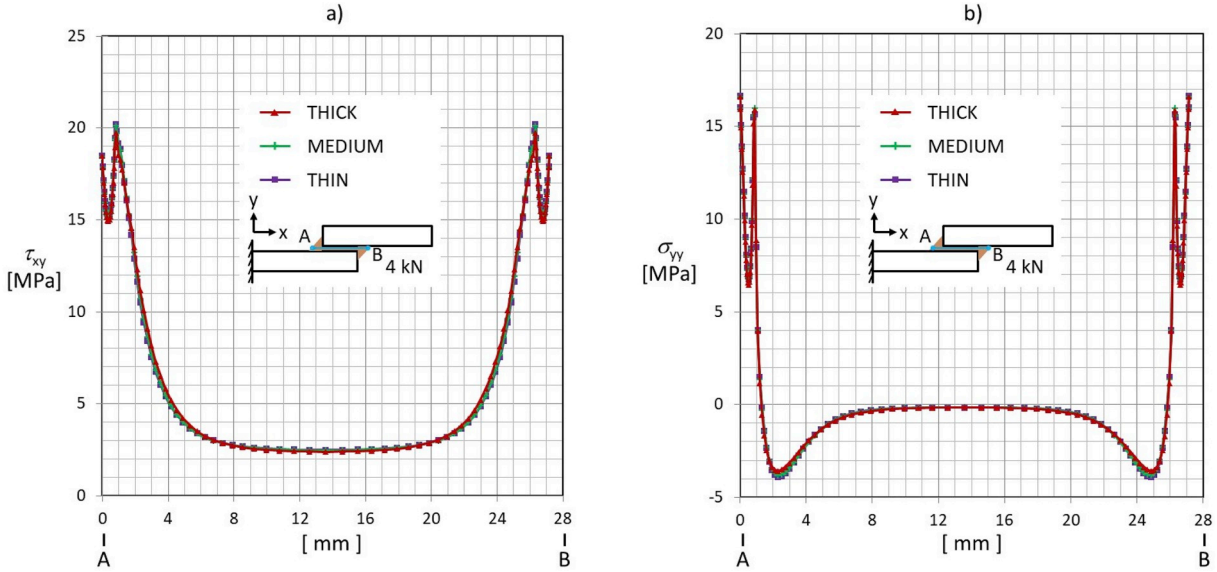

Fig. 14. Numerical comparison of a) shear stress (τ_{xy}) and b) peel stress (σ_{yy}) along the full bond line length including the spew region, at mid-width position.

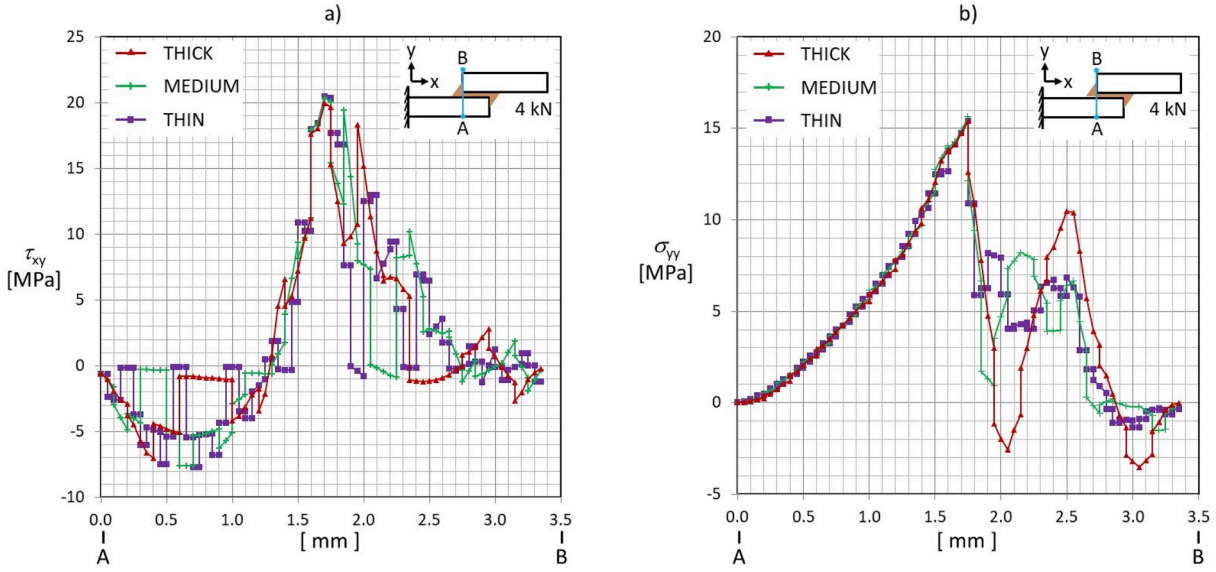

Fig. 15. Numerical comparison of a) shear stress (τ_{xy}) and b) peel stress (σ_{yy}) through the full overlap thickness, at mid-width position.

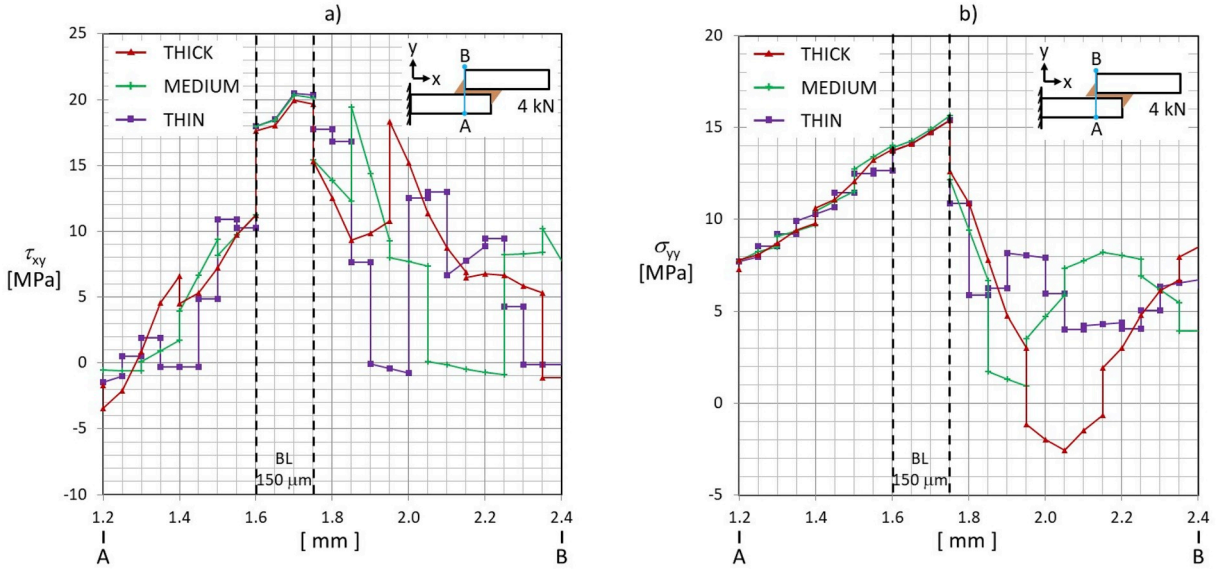

Fig. 16. Numerical comparison of a) shear stress (τ_{xy}) and b) peel stress (σ_{yy}) around the adhesive bond line, at mid-width position.

- Type III (P_{III} (x)): An equilibrium state between the mechanical and AE-energy
- Type IV (P_{IV} (x)): A decreasing behaviour which is related to the fact that the AE activity is greater than the material strain energy storing capability, so that the damage has reached a maximum

For a typical specimen of each configuration, the Sentry function is plotted over the load-displacement curve in Fig. 17. The beginning of the load-displacement curve, up to a displacement of 0.65 mm, is excluded here: An initial non-linearity in the load-displacement curves ("Toe") at the start of the test would lead to a large (Type II) drop, but does not correspond to any form of damage initiation.

A similar general trend is visible for all three different ply thickness configurations. The logarithmic plot starts with a (Type II) drop in case of MEDIUM and a more gentle (Type IV) in case of the THIN configuration. In all three configurations there is a slightly increasing trend (Type I) pronounced over the majority of the plot. In the MEDIUM configuration, this (Type I) trend changes into a (Type III) plateau.

With decreasing ply thickness, the length of this (Type I) trend, or in case of the MEDIUM the (Type III) plateau, increases, followed by a sudden drop of (Type II) and a subsequent decreasing behaviour of (Type IV) until final failure. This last Type IV is longer, in terms of displacement, for the THICK than the MEDIUM and it disappears for the THIN.

The initial (Type II) drop observed in the MEDIUM configuration as well as the less pronounced (Type IV) decrease in the THIN configuration, may be related to possible manufacturing defects inside the adhesive bond line. It is believed that those defects are significant in terms of acoustic energy in relation to the so far energy stored in the specimen but not significant enough in relation to the overall damage process. Further findings of the sentry function analysis will be discussed after presenting the results of the subsection hereafter.

5.2. Failure analysis

The numerical approach to derive the load at damage initiation was

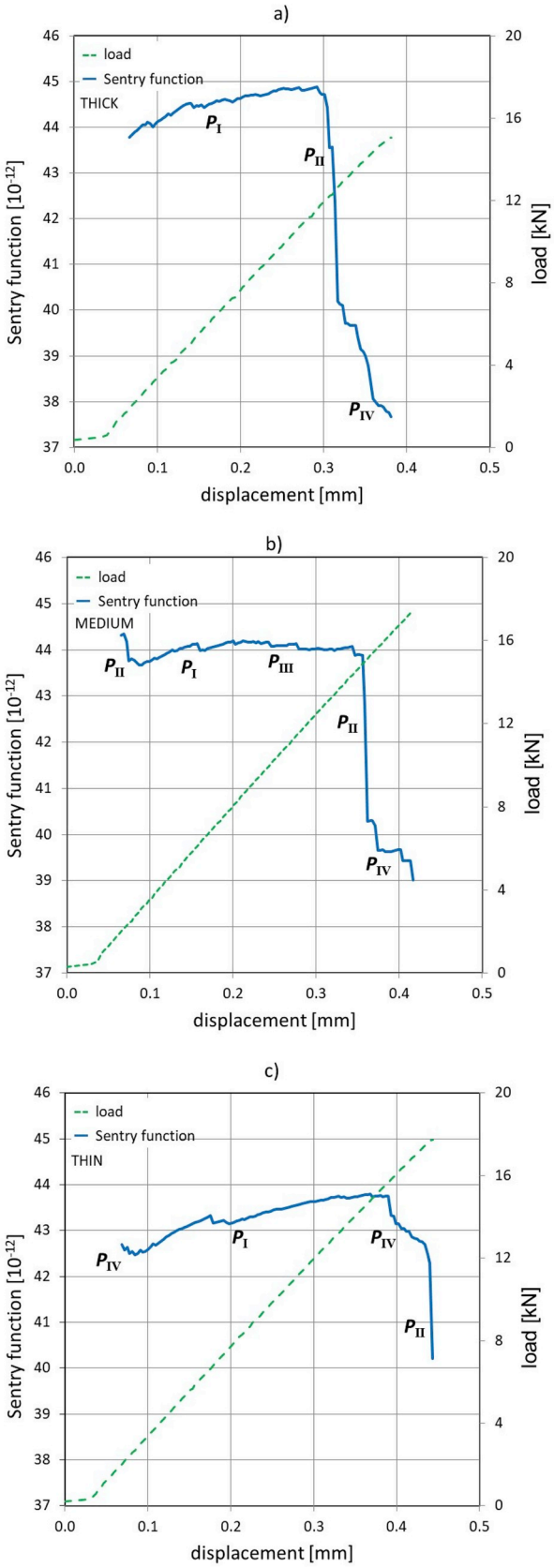

Fig. 17. Sentry function over load-displacement curve for different ply thickness configurations.

established by post-processing the stress tensor for each node. A set of user-defined subroutines was built to contain various failure criteria. For the adhesive, the von Mises as well as the Drucker-Prager yield criterion were used.

In the later, the study follows the approach of L.F.M. da Silva et al. [20], where the yield criterion can be expressed as

$$aq^b - p = p_t \tag{4}$$

The terms that appear in Equation (4) are defined as

$$a = \frac{1}{3(\beta - 1)\sigma_{yt}} \tag{5}$$

$$q = \sqrt{\frac{1}{2}\left[(\sigma_1 - \sigma_2)^2 + (\sigma_2 - \sigma_3)^2 + (\sigma_3 - \sigma_1)^2\right]} \tag{6}$$

$$b = 2$$

$$p = -\frac{1}{3}(\sigma_1 + \sigma_2 + \sigma_3) \tag{7}$$

$$p_t = \frac{\beta\sigma_{yt}}{3(\beta - 1)} \tag{8}$$

with b as the exponent parameter, σ_{yt} for the adhesive's yield stress in tension, β representing the ratio of yield stress in compression to the yield stress in tension and σ_1, σ_2 and σ_3 being the principal stresses at the element nodes. In this study, there were no experimental values available for the compressive yield stress of the chosen adhesive Hysol EA 9695™ 050K AERO. The β-value was chosen 1.45, based on values found in literature for adhesives with comparable Young's modulus and yield strength [11].

For the ply failure inside the composite, the 3D-invariant based criterion of Camanho et al. [21]. was used. The criterion distinguishes between fibre and matrix failure. In this criterion, the strength of a single UD-layer inside a stacking sequence varies with respect to its ply thickness and position within the sequence. This in-situ effect is incorporated, following the work of Camanho et al. [2]. The UD-properties in comparison with their elevated in-situ representative are shown in Table 6. The values show how much the values increase with respect to their position and thickness.

Fig. 18 and Table 7 present the comparison of experimental and numerical results. On the experimental side, the values for average lap shear strength (dark-blue) were directly provided by the load cell and the values for average shear stress at damage initiation (light-blue) were derived from cumulative AE-energy plots – see Table 4. On the numerical side, the stress tensor of the Abaqus-ODB was post-processed through a set of user-defined subroutines, containing the failure criteria.

The non-linear FE analysis indicates damage initiation inside the adhesive at lower loads than inside the composite. For all ply thicknesses, both Mises (dark-purple) and Drucker-Prager (light-purple) stress based criteria indicate a failure initiation inside the adhesive at lap shear stresses between 7.4 MPa and 8.7 MPa, which is at about 30% of the maximum load reached during experiments. Damage initiation inside the composite, given by the 3D-invariant based failure criteria (green), is at the same range as the failure inside the adhesive for the THICK configuration but at higher values for the MEDIUM and THIN configurations. Important to notice that, the failure inside the composite follows the trend of the experimental values, obtained by AE-signals, although at about 40% lower stresses. This discrepancy may be caused by the sensitivity of the failure analysis. The subroutine runs all nodes of the model and indicates failure as soon as the first node reaches a failure index › 1.001. The AE-sensors on the other hand are set to a minimum threshold for signal recording of 50 dB and it is believed that these two thresholds may not be comparable.

Following Camanho's approach, allowables for transverse matrix strength are enhanced due to the application of the in-situ theory [2].

Table 6
UD versus in-situ properties for NTPT Thinpreg™ 135, all values in [MPa].

	In-plane shear strength S_L	Transverse shear strength S_T	Transverse tensile strength Y_T	Transverse biaxial tensile strength Y_{BT}	Transverse compressive strength Y_C
UD/ply block	81[a]	35[b]	81[a]	50[c]	−255[b]
Double-THICK 0.40 mm INNER	99	43	128	88	−299
THICK 0.20 mm OUTER	85	37	81	50	−266
THICK 0.20 mm INNER	104	45	128	86	−310
MEDIUM 0.10 mm OUTER	104	45	114	73	−310
MEDIUM 0.10 mm INNER	126	54	180	130	−358
THIN 0.05 mm OUTER	126	54	161	109	−358
THIN 0.05 mm INNER	151	65	255	204	−408

[a] Based on material characterization tests, ASTM D3039/D3518/D6641 [7–9].
[b] TDS of NTPT Thinpreg™ 135 with HS40/T800 carbon fibers in 67 g/m^2 [11].
[c] Camanho et al. [2,21].

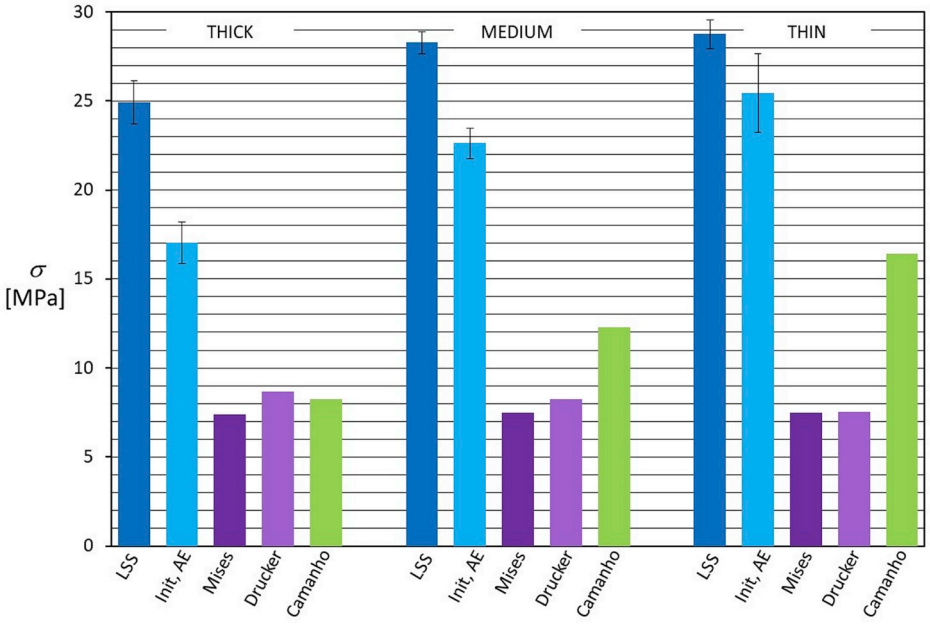

Fig. 18. Experimental average lap shear strength versus experimental and numerical average shear stress at damage initiation.

Therefore a decrease in ply thickness must consequently lead to first ply failure inside the composite at a higher load. This thought correlates with the observations of AE signals, which show that the sudden increase of cumulative acoustic energy occurs at higher loads when decreasing the ply thickness. The observation is also in agreement with recent studies of Amacher et al. [1] and Cugnoni et al. [6], who showed that a decrease in ply thickness postpones damage initiation and leads to higher fatigue life as well as impact resistance. In the FE analysis, stresses in the adhesive before damage initiation are almost identical in all three cases. So, a decrease in ply thickness would primarily affect the damage initiation inside the composite adherend.

Fig. 19 plots the failure indexes determined by post processing the nodal stresses from the FEM at the region of the overlap tip. The 3D model is reduced to a 2D illustration by plotting only the highest failure index of the (x,y) coordinate in the specimen's width direction (z-plane). Fig. 19 gives an idea where the damage onset is more likely to occur. Fig. 19 a) – c) show the failure indexes in the composite, for the three ply thicknesses a) THICK, b) MEDIUM, c) THIN at the corresponding load for damage initiation inside the composite. In all three cases, composite failure is indicated in the non-free adherend, nonetheless the location of the "hot-spots"(areas with higher FI) change with decreasing the ply thickness: from the interface ply on the THICK configuration to also inner plies in the THIN configuration. In case of the THIN configuration, in Fig. 19 c), a high failure index close to 1 is indicated in three different

Table 7
Average lap shear strength versus stress at damage initiation: Experimental (EXP) and numerical (NUM) approaches, all values in [MPa] (±standard deviation).

Configuration	σ_{LSS} EXP	$\sigma_{init,\ AE}$ EXP	Mises NUM	Drucker Prager NUM	Camanho NUM
THICK	24.9 (±1.2)	17.0 (±1.2)	7.4	8.7	8.3
MEDIUM	28.3 (±0.6)	22.6 (±0.9)	7.5	8.2	12.3
THIN	28.8 (±0.8)	25.4 (±2.2)	7.5	7.5	16.4

interfaces, which points towards the observations from the three fracture planes observed in final fracture surfaces in Fig. 9.

Fig. 19 d) presents the failure pattern inside the adhesive, based on the von Mises criterion. Here, the results for different ply thicknesses were very close to each other. Therefore the plot of the MEDIUM ply thickness is chosen to represent all three cases. The highest FI are located close to the upper adherend corner. This suggests that, smoothening the topology at this location might further decrease the "hot-spots" in the bondline.

The prediction of the damage onset location inside the composite matches the observations of the fracture surface analysis in subsection 3.4, where the fracture plane in case of the THIN configuration reached much deeper inside the composite adherend. However, the final fracture surfaces in Fig. 9 enable a glance at the last failure of the entire bonded joint, but do not tell about the location of damage initiation or propagation.

The result of the final fracture surfaces raise the question, how the crack could overcome several layers inside the composite, when reaching a sufficiently small ply thickness in the THIN configuration. From the experimental side of this study and the failure analysis shown in Fig. 19, it appears that decreasing the ply thickness favours multiple transverse matrix cracking, as in the THIN, instead of single in-plane delamination, as in the THICK and MEDIUM. The in-situ theory might help understanding: as the ply thickness decreases the matrix transverse crack initiates and progresses at higher loads. This allows, in the THIN configuration, that multiple transverse cracking can initiate and propagate simultaneously. In the final fracture surface, these concurrent

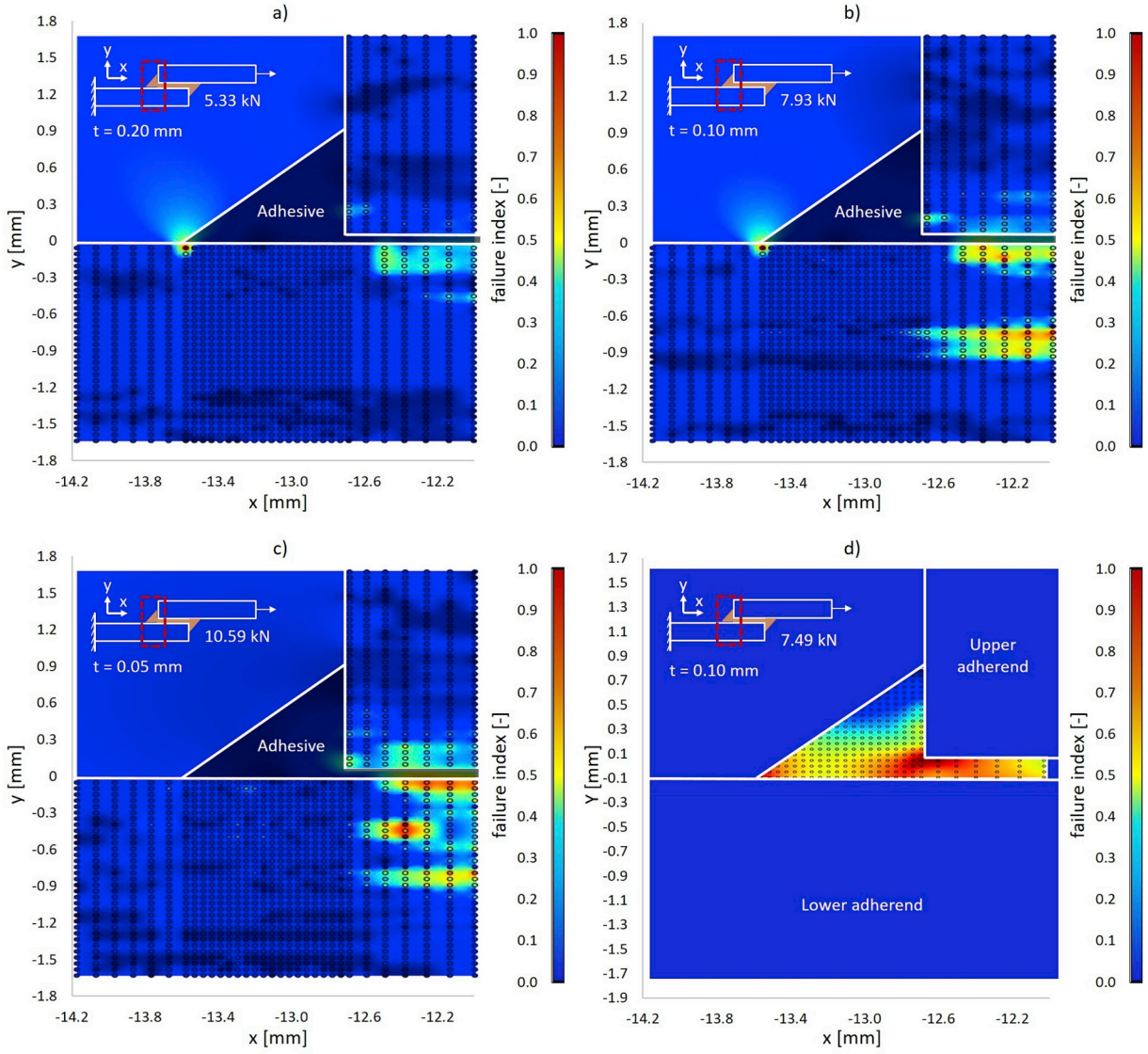

Fig. 19. Failure indexes (FI) at the region of the overlap tip for the load of damage initiation of the composite at the THICK (a), MEDIUM (b) and THIN (c) configuration (a, b, c only FI of the composite) and for the load of damage initiation at the adhesive bondline at the MEDIUM configuration (d) – only FI of the adhesive.

transverse cracks can be observed, connected by multiple delaminations. On the contrary, for THICK plies the transverse cracks occur at a lower load and rapidly propagate through the ply thickness, not giving enough room for other transverse cracks to occur and dissipate energy. This results in single transverse cracking and single in-plane delamination.

The numerical results indicate that the damage initiation occurs at a lower load inside the adhesive than inside the composite. The discrepancy raises the question, whether the experimental AE results are to be related to the composite failure alone. Both matrix and adhesive materials have very similar stiffness and density properties, and their location with respect to the position of the AE sensors is almost identical, so that the AE signal does not specifically tell, if a failure happens inside the matrix of the composite laminated adherend or inside the adhesive. However, when looking onto Fig. 4a)–c), the cumulative AE hits do indicate some form of damage in the early stage, before reaching the knee point of significant increase in acoustic energy release. It is believed, that the adhesive inside the bond line suffers early damage at low loads, which is captured by the Mises and Drucker-Prager criterion, before the Camanho criterion indicates damage initiation inside the composite, which correlates with the massive increase in cumulative acoustic energy in Fig. 4d)–f).

The location, where the Sentry function undergoes its sudden drop (Type II), can be related to the location of significantly increasing cumulative AE-energy, of Fig. 4d)–f). It is believed that this significant increase in acoustic energy (or sudden drop of the Sentry function), which occurs at higher displacement with decreased ply thickness, indicates the damage initiation inside the composite adherends. This result would meet the expectations based on previous studies on thin ply composites: A decrease in ply thickness postpones damage initiation to higher loads, while decreasing the damage tolerance of the composite until final failure [1,6]. The second part of this statement correlates to the experimental AE-results. The amount of cumulative AE energy after the point of damage initiation represents the last (Type IV) drop of the Sentry function and is significantly less pronounced with decreasing ply thickness.

Finally, a comparison of the joint configurations can be made, by correlating the load at damage initiation ($\sigma_{\text{init,AE}}$) and load at final failure (σ_{LSS}). The term "damage resistance" can be proposed as

$$D = 1 - \frac{\sigma_{init,AE}}{\sigma_{LSS}} \tag{9}$$

The values of Table 7 result in a damage resistance of 0.31 (±0.08) for the THICK, 0.20 (±0.04) for the MEDIUM, and 0.12 (±0.06) for the THIN configuration. Consequently, a decrease in ply thickness from the THICK to the THIN configuration is related to 61% lower damage resistance inside the composite adherend.

6. Conclusion

This study aims to explore the effect of the ply thickness on the damage initiation and final failure of CFRP bonded SLJ. Three different ply thickness configurations of 200 μm ("Thick"), 100 μm ("Medium") and 50 μm ("Thin") were tested under quasi-static tensile loading. Tests were monitored using AE-techniques to follow the damage events. An FE-analysis was performed to numerically simulate the experimental tests up to damage initiation. From the analysis of the results the following conclusions can be drawn:

- Decreasing the single ply thickness of laminated composite adherends increases the maximum load at final failure of the joint by 16% but postpones the event of damage initiation to a 47% higher load.
- The final fracture surface is dominated by failure inside the composite. A decrease in ply thickness from 200 μm to 50 μm leads, on average, to a decrease in fracture surface from 118% to 99% of initial overlap area.
- A non-linear finite element analysis up to damage initiation indicates no noticeable difference in maximum shear (τ_{12}) or peel (σ_{22}) stress inside the adhesive when varying the ply thickness of the composite adherends.
- Adhesive failure is indicated at around 30% of maximum load, always at the interface of the outermost adherend layer to the adhesive, independently from ply thickness.
- Based on Camanho's ply failure criteria, damage onset in the composite is likely to occur at the same load level as in the adhesive, in case of the THICK configuration and at 50% higher load level in case of the THIN configuration. The location of composite failure changes from the ply interface towards the mid thickness of the composite adherend with decreasing ply thickness, due to the fact, that the 3D-invariant based criterion takes into account the in-situ effect of ply position and thickness.
- The use of thin plies in composite bonded joints leads to an enhancement of joint strength up to damage initiation but results in a more sudden damage progression till final failure.
- Defining damage resistance of the joint as the ratio of average shear stress between damage onset and final failure, the decrease of ply thickness from 200 μm to 50 μm in this study leads to a decrease in damage resistance of about 61%.

Data availability

The data required to reproduce these findings are available to download from http://doi.org/10.4121/uuid:04ba3dd6-075f-4543-a14f-ec406bd9163e.

Declaration of competing interest

The authors declare that they have no known competing financial interests or personal relationships that could have appeared to influence the work reported in this paper.

Acknowledgement

This work has been funded by the Netherlands Organisation for Scientific Research (NWO), project number 14366.

References

[1] Amacher R, Cugnoni J, Botsis J, Sorensen L, Smith W, Dransfeld C. Thin ply composites: experimental characterization and modelingof size-effects. Compos Sci Technol 2014;101:121–32.
[2] Camanho PP, Dávila CG, Pinho ST, Iannucci L, Robinson P. Prediction of in situ strengths and matrix cracking in composites under transverse tension and in-plane shear. Composites Part A 2006;37:165–76.
[3] Sihn S, Kim RY, Kawabe K, Tsai SW. Experimental studies of thin-ply laminated composites. Compos Sci Technol 2007;67:996–1008.
[4] Yokozeki T, Aoki Y, Ogasawara T. Experimental characterization of strength and damage resistance properties of thin-ply carbon fiber/toughened epoxy laminates. Compos Struct 2008;82:382–9.
[5] Arteiro A, Catalanotti G, Melro AR, Linde P, Camanho PP. Micro-mechanical analysis of the in situ effect in polymer composite laminates. Compos Struct 2014;116:827–40.
[6] Cugnoni J, Amacher R, Kohler S, Brunner J, Kramer E, Dransfeld C, Smith W, Scobbie K, Sorensen L, Botsis J. Towards aerospace grade thin-ply composites: effect of ply thickness, fiber, matrix and interlayer toughening on strength and damage tolerance. Compos Sci Technol 2018;168:467–77.
[7] ASTM-D3039M. Standard test method for tensile properties of polymer matrix composite materials. West Conshohocken, PA, USA: ASTM International, American Society for Testing and Materials; 2014.
[8] ASTM-D3518M. Standard test method for in-plane shear response of polymer matrix composite materials by tensile test of a ±45° laminate. West Conshohocken, PA, USA: ASTM International, American Society for Testing and Materials; 2013.
[9] ASTM-D6641M. Standard test method for compressive properties of polymer matrix composite materials using a combined loading compression test fixture. West Conshohocken, PA, USA: ASTM International, American Society for Testing and Materials; 2014.
[10] Material datasheet: Thinpreg™ 135. NTPT; 2017.

[11] Teixeira de Freitas S, Sinke J. Failure analysis of adhesively-bonded metal-skin-to-composite-stiffener: effect of temperature and cyclic loading. Compos Struct 2017; 166:27–37.
[12] datasheet Material. Scotch-Weld™ structural adhesive film AF, vols. 163–2; 2009.
[13] Kaw K. Mechanics of composite materials. Boca Raton: Taylor & Francis; 2006.
[14] ASTM-D5868. Standard test method for lap shear adhesion for fiber reinforced plastic (FRP) bonding. West Conshohocken, PA, USA: ASTM International, American Society for Testing and Materials; 2014.
[15] Ultraviolet-ozone surface treatment. Three Bond Technical News; 1987.
[16] Poulis JA. Small cylindrical adhesive bonds. PhD thesis. The Netherlands: Technical University Delft; 1993, ISBN -90-370-0082-7. p. 39–62.
[17] Teixeira de Freitas S, Zarouchas D, Poulis JA. The use of acoustic emission and composite peel tests to detect weak adhesion in composite structures. J Adhes 2018;94:743–66.
[18] Kupski J, Teixeira de Freitas S, Zarouchas D, Benedictus R, Camanho PP. Composite layup effect on the failure mechanism of single lap bonded joints. Compos Struct 2019;217:14–26.
[19] Saeedifar M, Fotouhi M, Najafabadi M, Toudeshky H, Minak G. Prediction of quasi-static delamination onset and growth in laminated composites by acoustic emission. Composites Part B 2016;85:113–22.
[20] da Silva LFM, Rodrigues TNSS, Figueiredo MAV, de Moura MFSF, Chousal JAG. Effect of adhesive type and thickness on the lap shear strength. J Adhes 2007;82: 1091–115.
[21] Camanho PP, Arteiro A, Melro AR, Catalanotti G, Vogler M. Three-dimensional invariant-based failure criteria for fibre-reinforced composites. Int J Solids Struct 2015;55:92–107.